



饱和土有限应变弹塑性本构模型研究

翁天赐, 熊勇林, 韩哲

Finite strain elastoplastic constitutive model of saturated soil

WENG Tianci, XIONG Yonglin, and HAN Zhe

在线阅读 View online: <https://doi.org/10.16030/j.cnki.issn.1000-3665.202404002>

中文核心期刊

CSCD核心期刊

中科双效期刊

中国科技核心期刊

Caj-cd规范获奖期刊

您可能感兴趣的其他文章

Articles you may be interested in

基于有限元软件自定义本构模型的膨胀土边坡降雨入渗分析

An analysis of rainfall infiltration of expansive soil slope based on the finite element software custom constitutive model
饶鸿, 王金淑, 赵志明, 吴光, 冯涛 水文地质工程地质. 2021, 48(1): 154–162

高应力区岩石统计损伤本构模型研究

A study of the statistical damage constitutive model of rock in high stress areas
贾逸, 魏良帅, 黄安邦, 和铭, 黄细超, 蓝康文 水文地质工程地质. 2019, 46(2): 118–118

水-岩作用下粉砂质泥岩含水损伤本构模型

Constitutive model of water-damaged silty mudstone under water-rock interactions
李安润, 邓辉, 王红娟, 郑瀚, 荀晓峰, 潘远阳 水文地质工程地质. 2021, 48(2): 106–113

一种基于弹性能释放率的岩石新型统计损伤本构模型

A statistical damage constitutive rock model based on elastic energy release rate
刘文博, 孙博一, 陈雷, 张树光 水文地质工程地质. 2021, 48(1): 88–95

基于非线性损伤理论的改进CVISC模型及其在FLAC3D中实现

A non-linear damage rheological constitutive model and its application to a giant slow-moving landslide
蒋树, 文宝萍, 蒋秀姿, 李瑞冬, 赵成 水文地质工程地质. 2019, 46(1): 56–56

膨胀土边坡非饱和渗流及渐进性破坏耦合分析

A coupling analysis of unsaturated seepage and progressive failure of an expansive soil slope
陈亮胜, 韦秉旭, 廖欢, 张寒冰 水文地质工程地质. 2020, 47(4): 132–140



关注微信公众号, 获得更多资讯信息

DOI: [10.16030/j.cnki.issn.1000-3665.202404002](https://doi.org/10.16030/j.cnki.issn.1000-3665.202404002)

翁天赐, 熊勇林, 韩哲. 饱和土有限应变弹塑性本构模型研究 [J]. 水文地质工程地质, 2025, 52(2): 94-103.
WENG Tianci, XIONG Yonglin, HAN Zhe. Finite strain elastoplastic constitutive model of saturated soil[J]. Hydrogeology & Engineering Geology, 2025, 52(2): 94-103.

饱和土有限应变弹塑性本构模型研究

翁天赐, 熊勇林, 韩 哲
(宁波大学岩土工程研究所, 浙江 宁波 315211)

摘要: 在城市地下工程的建设过程中, 土体普遍处于饱和状态, 而众多地下工程事故的发生与饱和土体的大变形行为紧密相连, 但目前大部分本构模型都建立在小应变条件下。为了深入揭示饱和土体的大变形力学特性, 本研究以有限应变理论为基础, 结合超弹性模型与修正剑桥模型, 引入上下负荷屈服面的概念来描述土体的超固结特性和结构性。利用具有数值计算优势的返回映射算法, 求解本构模型的非线性响应, 并推导出能够加速计算收敛并提高计算精度的一致切线刚度矩阵。在主应力空间内, 建立了一个能够同时考虑结构性、超固结特性以及大变形等力学特性的饱和土有限应变弹塑性本构模型。通过对试验数据与模型计算结果, 验证了所提出本构模型的准确性。进一步通过模拟等固压三轴排水剪切试验和三轴固结试验, 分别探讨了初始超固结比、初始结构性、超固结控制参数和结构性控制参数对土体力学特性行为的影响。结果表明: (1)随着超固结比增大, 土体峰值强度逐渐增大, 但最终体变由剪缩转为剪胀行为; (2)随着土体初始结构性的增强, 土体的峰值强度显著提高, 且应变软化的程度也随之增加; (3)超固结控制参数的增大或结构性控制参数的减小, 土体峰值强度均有所提升。研究结果为解决大变形工程中的问题提供了新的思路和方法, 具有重要的工程应用价值。

关键词: 大变形; 超固结; 结构性; 有限应变; 弹塑性; 本构模型

中图分类号: TU43 文献标志码: A 文章编号: 1000-3665(2025)02-0094-10

Finite strain elastoplastic constitutive model of saturated soil

WENG Tianci, XIONG Yonglin, HAN Zhe
(Institute of Geotechnical Engineering, Ningbo University, Ningbo, Zhejiang 315211, China)

Abstract: During the construction of urban underground engineering projects, soils are typically in a saturated state, and many underground engineering accidents are closely related to the large deformation behavior of saturated soils. However, most constitutive models are developed under small strain conditions. To better understand the mechanical characteristics of large deformation in saturated soils, this study applied finite strain theory, combining hyper-elastic and modified Cambridge models. The concept of subloading and superloading yield surfaces was introduced to describe the characteristics of overconsolidation and structure of soils. Utilizing the advantages of numerical computation, a return mapping algorithm was employed to solve the nonlinear response of the constitutive model and derive a consistent tangent stiffness matrix to accelerate convergence and improve computational accuracy. In the principal stress space, a finite strain elastoplastic constitutive model for saturated soils is established, which simultaneously considering structural characteristics, overconsolidation properties, and large deformation mechanical behaviors. Through comparison between experimental data and

收稿日期: 2024-04-01; 修订日期: 2024-07-17 投稿网址: www.swdzgcdz.com

基金项目: 浙江省自然科学基金项目(LY19E080012)

第一作者: 翁天赐(1999—), 男, 硕士研究生, 主要从事岩土数值计算方面的研究。E-mail: 1427058793@qq.com

通讯作者: 熊勇林(1986—), 男, 博士, 副教授, 主要从事岩土材料本构模型及数值分析方面的研究。E-mail: xiongyonglin@nbu.edu.cn

model calculations, the accuracy of the constitutive model is verified. Additionally, the study investigated the effects of initial overconsolidation ratio, initial structural characteristics, overconsolidation control parameters, and structural control parameters on soil mechanical behavior by simulating isotropic triaxial drained shear tests and triaxial consolidation tests. The results indicate that with increasing overconsolidation ratio, the peak strength of the soil gradually increases, but the final volumetric behavior transitions from shear compaction to shear dilation. As the initial structural characteristics of the soil strengthen, the peak strength significantly increases, and the degree of strain softening also increases accordingly. Increasing the overconsolidation control parameter or reducing the structural control parameter both lead to an increase in the peak strength of the soil.

Keywords: large deformation; overconsolidation; structural; finite strain; elastoplastic; constitutive model

在我国城市化快速发展的今天,城市土地资源短缺的矛盾越来越大,对地下空间进行开发已经成为一种必然的选择^[1]。在城市地下工程建设中,土体普遍处于饱和状态,而许多地下工程事故都与饱和土体的大变形行为密切相关^[2-3]。因此,开展饱和土体的大变形力学特性研究,对工程实践有着十分重要的意义。

影响土水特性的因素有很多,包括土的矿物成分^[4-5]、应力历史^[6]、应力路径^[7]、初始孔隙比^[8-9]等。目前为止,已有众多学者对饱和土的力学特性进行了深入研究,在试验与理论研究上已有较大进展,提出了多种土体本构模型,为地质灾害防治工作提供了指导性意见^[10-12]。刘青灵等^[13]建立了土壤全基质吸力段的土-水特征模型;李吴刚等^[14]结合修正剑桥模型推导了三轴应力状态下结构性土的本构模型;Chakraborty 等^[15]建立了双屈服面模型;汪华斌等^[16]对花岗岩残积土开展了一系列三轴试验,发现结构性花岗岩残积土的原状土和重塑超固结土均表现出明显的剪胀性,应力应变曲线均出现应变软化;孔令伟等^[17]通过对广东湛江地区强结构性黏土的研究,发现原状土到重塑土的转变过程是黏聚力和内摩擦角在土体内部相互消长的过程,强结构性黏土在结构屈服前的强度指标具有较强应力路径依赖性;祝恩阳等^[18-19]提出移动正常固结线的概念,并用移动正常固结线代替正常固结线作为参考线,将统一硬化模型拓展为可描述土结构性的结构性土统一硬化模型;路德春等^[20-21]基于特征应力的概念,采用修正特征应力空间中的倾斜屈服面,综合考虑土的各项异性和非正交流动性,建立了横观各向同性黏土的非正交弹塑性本构模型,该模型可退化为修正剑桥模型;郭万里等^[22]以剑桥模型剪胀公式为依据,引进曲线形态调节因式,推导出一种新的剪胀公式,并发展了一种适合于粗颗粒土的广义塑性模型;张玉伟等^[23]在改进修正剑桥模型的基础上,将结

构参数引入到初始屈服面,并采用屈服面转动法,将各向异性参数引入到黄土的各向异性中,从而构建能够反映黄土结构及各向异性特征的修正剑桥模型。

以上本构模型大多基于小变形理论,但小变形理论中通常采用次弹性模型,这会导致能量的不合理耗散,而有限应变理论中采用超弹性模型,能保证了储存能量的守恒^[24]。且有限应变理论中采用 Hashiguchi^[25]所提出的双对数 $\ln v - \ln P$ (v 为体积, P 为平均主应力) 压缩曲线,相较于单对数 $v - \ln P$ 压缩曲线,在试样承受较大的应力值 P 时,双对数压缩曲线能保证 v 不会为负,而单对数压缩曲线则会出现 v 为负值的情况,显然双对数 $\ln v - \ln P$ 压缩曲线更为合理,应用范围更加广泛,且能更好地描述土体的大变形行为。因此许多学者基于有限应变理论进行本构模型研究,如 Borja 等^[26-27]基于变形梯度的有限应变理论框架,将超弹性储能函数与临界状态塑性模型相结合,并提出了一种计算非线性弹性剑桥模型的隐式应力积分算法,建立了有限应变剑桥模型;祝恩阳等^[19]基于基尔霍夫应力不变量建立了一种可以描述非饱和土压缩和坍塌特性的弹塑性本构模型,该模型既能预测非饱和土的大变形行为,也可描述非饱和土的水力特性;胡小荣等^[28]以三剪统一强度准则为破坏准则,利用等量替代法和坐标平移法分别推导出正常饱和黏性土的三剪破坏应力比,结合有限变形理论和修正剑桥模型建立了正常饱和黏性土三剪有限变形弹塑性本构模型。

总览上述文献所提本构模型,目前可以较为全面的描述超固结、结构性土大变形行为的模型较少。本文基于有限应变理论,结合超弹性模型、双对数压缩曲线、上下负荷面概念和返回映射算法,在主应力空间建立了一个考虑超固结、结构性、大变形的饱和土有限应变弹塑性本构模型,通过与试验数据的比较,验证本文所建立本构模型的准确性。

1 饱和土有限应变弹塑性本构模型

1.1 超弹性模型

超弹性模型在加载过程中出现塑性变形会产生硬化,也能描述大变形问题,常用于分析多孔介质材料。因此,本文采用超弹性模型描述土体的力学性质,并应用压力相关的体积和剪切模量的超弹性模型描述弹性响应。

超弹性储能函数(W)定义为弹性体积应变(ε_v^e)和弹性剪切应变(ε_s^e)的函数:

$$W(\varepsilon_v^e, \varepsilon_s^e) = \tilde{W}(\varepsilon_v^e) + \frac{3}{2}\mu^e \varepsilon_s^{e2} \quad (1)$$

$$\tilde{W}(\varepsilon_v^e) = -P_{\text{ref}}\hat{\kappa} \exp \Omega \quad (2)$$

$$\Omega = -\frac{\varepsilon_v^e - \varepsilon_{v,\text{ref}}^e}{\hat{\kappa}} \quad (3)$$

$$\mu^e = \mu_0 + \frac{\alpha \tilde{W}(\varepsilon_v^e)}{\hat{\kappa}} \quad (4)$$

式中: $\tilde{W}(\varepsilon_v^e)$ ——各向同性加载时的储能函数;

μ^e ——弹性剪切模量/kPa;

$\varepsilon_{v,\text{ref}}^e$ ——在参考应力 P_{ref} 下的弹性体积应变;

$\hat{\kappa}$ ——有限应变条件下的弹性回弹指数;

μ_0 ——初始弹性剪切模量/kPa;

α ——弹性剪切模量参数。

由式(4)可知当 α 为 0 时, μ^e 为恒定弹性剪切模量;而当 α 非 0 时, μ^e 为与压力相关的弹性剪切模量。根据式(1)计算基尔霍夫平均主应力(P)和基尔霍夫偏应力(Q),其表达式分别为:

$$P = \frac{\partial W(\varepsilon_v^e, \varepsilon_s^e)}{\partial \varepsilon_v^e} = P_{\text{ref}} \exp \Omega \left[1 + \frac{3\alpha}{2\hat{\kappa}} \varepsilon_s^{e2} \right] \quad (5)$$

$$Q = \frac{\partial W(\varepsilon_v^e, \varepsilon_s^e)}{\partial \varepsilon_s^e} = 3(\mu_0 - \alpha P_0 \exp \Omega) \varepsilon_s^e \quad (6)$$

本文以下所提到的 P 和 Q 若无特别说明,均指为基尔霍夫平均主应力和基尔霍夫偏应力。有限应变和小应变的应力与矩阵转换为:

$$\boldsymbol{\beta} = J \cdot \boldsymbol{\sigma}, \quad \mathbf{D}^e = J \cdot \mathbf{C}^e \quad (7)$$

$$J = \det \mathbf{F} = \frac{v}{v_0} = \frac{1+e}{1+e_0} \quad (8)$$

式中: $\boldsymbol{\beta}$ ——基尔霍夫应力/kPa;

$\boldsymbol{\sigma}$ ——柯西应力/kPa;

\mathbf{D}^e ——有限应变弹性刚度矩阵;

\mathbf{C}^e ——小应变弹性刚度矩阵;

J ——变形速率张量 \mathbf{F} 的雅可比行列式;

v, e ——现在时刻(t)的比体积、孔隙比;

v_0, e_0 ——参考时刻(t_0)的比体积、孔隙比。

1.2 屈服函数

有限应变中采用双对数 $\ln v - \ln P$ 压缩曲线,其表达式为:

$$\ln v = \ln v_{\text{ref}} - \lambda \ln \frac{P}{P_{\text{ref}}} \quad (9)$$

式中: v_{ref} ——参考应力下的比体积;

λ —— $\ln v - \ln P$ 下的压缩指数。

由式(9)可知,在有限应变条件下,试样各向同性固结的有限体积应变($\varepsilon_{v(c)}$)为:

$$\varepsilon_{v(c)} = \ln \frac{v}{v_0} = \ln v - \ln v_0 = -\hat{\lambda} \ln \frac{P}{P_0} \quad (10)$$

式中: P_0 ——初始平均主应力/kPa;

$\hat{\lambda}$ ——有限应变压缩指数。

有限应变与小应变参数可相互转化^[24],其表达式如下:

$$\hat{\lambda} = \frac{\tilde{\lambda}}{1-\tilde{\lambda}}, \quad \hat{\kappa} = \frac{\tilde{\kappa}}{1-\tilde{\kappa}} \quad (11)$$

式中: $\tilde{\lambda}$ ——小应变压缩指数;

$\hat{\kappa}$ ——有限应变回弹指数;

$\tilde{\kappa}$ ——小应变回弹指数。

在有限应变条件下,试样各向同性固结时弹性体积应变($\varepsilon_{v(c)}^e$)为:

$$\varepsilon_{v(c)}^e = \varepsilon_{v0}^e - \hat{\kappa} \ln \frac{P}{P_0} \quad (12)$$

式中: ε_{v0}^e ——试样在平均主应力为 P_0 时产生的弹性体积应变。

结合式(10)(12)可知,试样各向同性固结时塑性体积应变($\varepsilon_{v(c)}^p$)为:

$$\varepsilon_{v(c)}^p = \varepsilon_{v(c)} - \varepsilon_{v(c)}^e = -(\hat{\lambda} - \hat{\kappa}) \ln \frac{P}{P_0} - \varepsilon_{v0}^e \quad (13)$$

选择屈服面为修正剑桥模型椭圆屈服面,由剪切引起的塑性体积应变($\varepsilon_{v(d)}^p$)为:

$$\varepsilon_{v(d)}^p = -(\hat{\lambda} - \hat{\kappa}) \ln \left(1 + \frac{Q^2}{M^2 P^2} \right) \quad (14)$$

式中: M ——临界状态应力比。

结合式(13)(14)推导出有限应变条件下正常固结饱和土的屈服函数为:

$$f = (\hat{\lambda} - \hat{\kappa}) \left[\ln \frac{P}{P_0} + \ln \left(1 + \frac{Q^2}{M^2 P^2} \right) \right] + \varepsilon_{v0}^e + \varepsilon_{v(d)}^p \quad (15)$$

式中: ε_v^p ——塑性体积应变, $\varepsilon_v^p = \varepsilon_{v(c)}^p + \varepsilon_{v(d)}^p$ 。

为了更好地描述土的结构性和超固结性,引入上

1.4 一致切线刚度矩阵

在解决非线性响应问题时,通常需要对系统进行一致线性化以获得最佳收敛结果,同时也能提高计算效率。接下来在主应力空间内推导一致切线刚度矩阵。

对式(22)进行全微分可得:

$$d\boldsymbol{\varepsilon}_{n+1}^e = d\boldsymbol{\varepsilon}_{n+1} - \frac{\Delta\gamma}{J} \partial_{\sigma\sigma}^2 f_{n+1} d\sigma_{n+1} - \frac{1}{J} \partial_\sigma f_{n+1} d\Delta\gamma_{n+1} \quad (26)$$

根据应力应变关系可知:

$$d\sigma_{n+1} = \frac{1}{J} \mathbf{D}_{n+1}^e d\boldsymbol{\varepsilon}_{n+1}^e \quad (27)$$

将式(27)代入式(26)中,可得:

$$d\sigma_{n+1} = \boldsymbol{\Xi}_{n+1} \left(d\boldsymbol{\varepsilon}_{n+1} - \frac{1}{J} \partial_\sigma f_{n+1} d\Delta\gamma_{n+1} \right) \quad (28)$$

$$\boldsymbol{\Xi}_{n+1} = \left[J(\mathbf{D}_{n+1}^e)^{-1} + \frac{\Delta\gamma}{J} \partial_{\sigma\sigma}^2 f_{n+1} \right]^{-1} \quad (29)$$

$$\mathbf{D}_{n+1}^e = \frac{\partial^2 W}{\partial \boldsymbol{\varepsilon}_{n+1}^e \partial \boldsymbol{\varepsilon}_{n+1}^e} \quad (30)$$

对式(20)和式(21)进行全微分可得:

$$dR_{n+1} = -\frac{m R_{n+1} \ln R_{n+1}}{R_{n+1} + m\Delta\gamma} d\Delta\gamma \quad (31)$$

$$dR_{n+1}^* = \frac{m^* R_{n+1}^* (1 - R_{n+1}^*)}{1 - m^* (1 - 2R_{n+1}^*)} d\Delta\gamma \quad (32)$$

根据式(26)可知,塑性体积应变的表达式为:

$$d\varepsilon_v^p = \Delta\gamma \frac{\delta}{J} \partial_{\sigma\sigma}^2 f_{n+1} d\sigma_{n+1} + \frac{\delta}{J} \partial_\sigma f_{n+1} d\Delta\gamma_{n+1} \quad (33)$$

式中: δ ——列向量, $\delta = (1, 1, 1)^T$ 。

与剑桥模型一样,采用联合流动法则,根据一致性条件可知:

$$df_{n+1} = (\partial_\sigma f_{n+1})^T d\sigma_{n+1} + \partial_R f_{n+1} dR_{n+1} + \partial_{R^*} f_{n+1} dR_{n+1}^* + \partial_{\varepsilon_v^p} f_{n+1} d\varepsilon_v^p = 0 \quad (34)$$

将式(28)、(31)—(33)代入到式(34)中,可得:

$$d\Delta\gamma_{n+1} = N \cdot \boldsymbol{\Xi}_{n+1} \cdot d\boldsymbol{\varepsilon}_{n+1} / \mathbf{D} \quad (35)$$

$$N = (\partial_\sigma f_{n+1})^T + \frac{\Delta\gamma}{J} \delta \partial_{\sigma\sigma}^2 f_{n+1} \quad (36)$$

$$\mathbf{D} = \frac{N \cdot \boldsymbol{\Xi}_{n+1} \cdot \partial_\sigma f_{n+1}}{J} - \frac{\delta \cdot \partial_\sigma f_{n+1}}{J} - \frac{\partial_R f_{n+1} dR_{n+1} - \partial_{R^*} f_{n+1} dR_{n+1}^*}{J} \quad (37)$$

将式(35)回代式(26)中即可得到一致切线刚度矩阵的表达式:

$$\frac{d\sigma_{n+1}}{d\boldsymbol{\varepsilon}_{n+1}} = \boldsymbol{\Xi}_{n+1} - \boldsymbol{\Xi}_{n+1} \cdot \partial_\sigma f_{n+1} \cdot N \cdot \boldsymbol{\Xi}_{n+1} / J \cdot \mathbf{D} \quad (38)$$

2 本构模型的对比验证

基于所建立的饱和土有限应变弹塑性本构模型,用 MATLAB 软件编制了应变控制和应力控制的常规固结、三轴固结和三轴排水剪切试验的计算程序。根据试验的初始条件确定初始的模型参数,并将模型计算结果与试验结果进行对比验证。

本文采用 Ye 等^[30]对饱和原状土的常规固结和三轴排水剪切试验的试验数据进行对比验证。用于模拟的模型参数如表 1 所示。室内三轴剪切试验中,对每层原状土进行了等围压下的排水剪切试验,其围压大小如表 2 所示。图 2 所示为饱和原状土常规固结试验与模型模拟的对比情况,可以看出,模拟结果与试验结果高度吻合,显示出较好的一致性。图 3 所示为多层土不同围压条件下的偏应力-轴向应变曲线和体积应变-轴向应变曲线。从图 3 可以看出各层土偏应力轴向位移曲线模拟效果较好,但由图 3(b)中可知,模型对超固结土的剪胀特性有些高估。总体来说,本研究所提出的模型,能够针对同一土体,采用一套参数,能够较好地同时模拟固结与三轴剪切试验结果,但是计算的体积变形与试验结果相差有点大,这主要是由于本文采用了联合流动法则,后续研究拟选用合适的塑性势函数对土体塑性变形进行计算。

表 1 饱和原状土的模型参数
Table 1 Model parameters of saturated undisturbed soil

土层	参数										
	λ	$\hat{\kappa}$	μ_0/kPa	α	M	$P_{\text{ref}}/\text{kPa}$	V_{ref}	m	m^*	R	R^*
层 2	0.061	0.005	10 000	0	1.20	98	1.79	0.05	1.000 0	0.105	1.00
层 3	0.078	0.008	20	360	1.30	98	2.04	0.10	0.002 0	0.186	0.30
层 4	0.100	0.010	2 000	360	1.38	98	1.94	0.05	0.003 3	0.128	0.41

3 模型参数讨论

通过以上试验的模拟,该模型数值计算结果能与

试验数据较好地拟合,验证了所提本构模型的正确性。接下来进一步研究相关模型参数的变化对模型性能的影响。以下算例为等围压排水剪切试验和三

表 2 饱和原状土三轴剪切试验围压

Table 2 Confining pressure of saturated undisturbed soil under triaxial shear test

土层	围压/kPa		
层 2	100	200	300
层 3	100	200	300
层 4	100	200	400

轴固结试验的模型模拟, 其模型参数如表 3 所示。

算例 1—3 的三轴排水剪切试验计算结果如图 4 所示, 从图中可知: 对于初始超固结比较小的土样, 其表现为应变硬化, 初始超固结比较大的土样, 其表现为先应变硬化而后应变软化; 初始超固结比较小的土样产生剪缩, 初始超固结比较大的土样先发生剪缩后逐渐发生剪胀。算例 4—5 的三轴排水剪切试验计算结果如图 5 和图 6 所示, 从图中可以看出: 随着超固结控制参数 m 的增大, 土体的峰值强度有所上升, 出现峰值强度对应的轴向应变逐渐减小。以上算例的三轴固结试验计算结果如图 7 所示, 图中平均净应力为三个主应力的平均值。由图中可知: 不同初始超固结比的 $\ln v - \ln P$ 曲线最终都与正常固结线 (normal consolidation line, NCL) 重合; 超固结控制参数越大, $\ln v - \ln P$ 曲线靠近 NCL 的速度越快。算例 6—7 的三轴排水剪切试验计算结果如图 5 和图 6 所示, 从图中可知: 随着

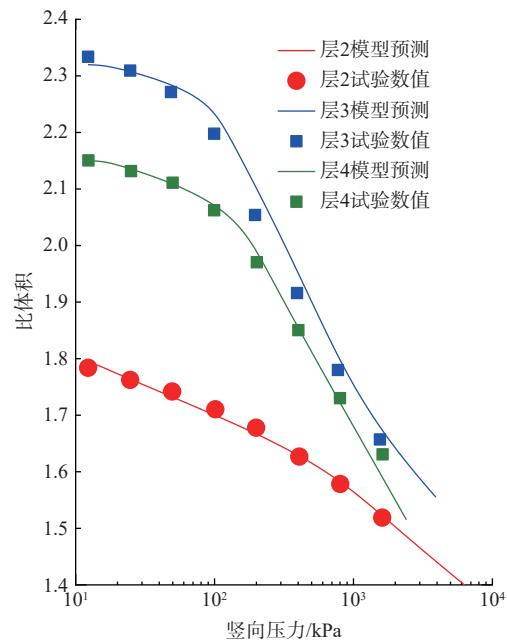


图 2 饱和原状土常规固结试验结果与模拟值对比

Fig. 2 Comparison between conventional consolidation test results and simulated values of saturated undisturbed soil

土体结构性 R^* 的增加, 土体峰值强度显著提升, 其应变软化的程度也有所增大。算例 8—9 的三轴排水剪切试验计算结果如图 5 和图 6 所示, 由图中可知: 结构性控制参数 m^* 越小, 结构性消散越慢, 土体的峰值强

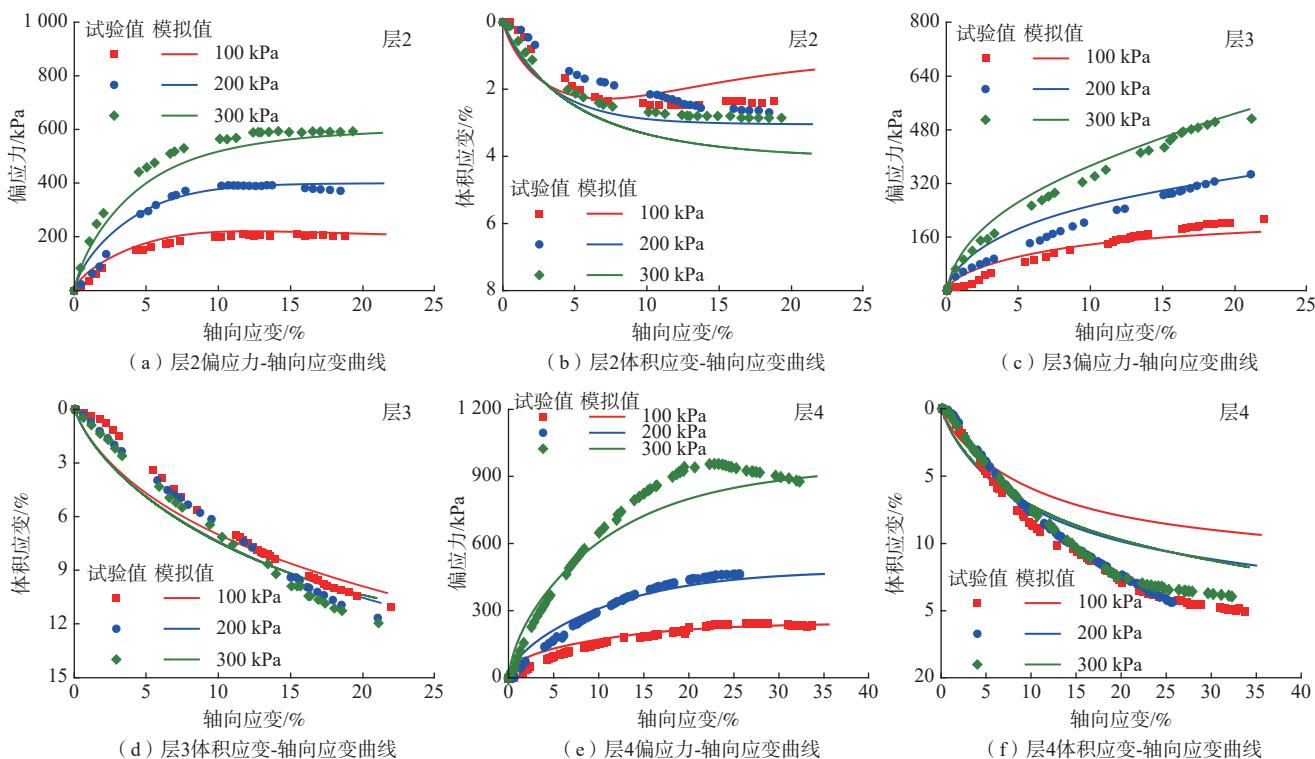
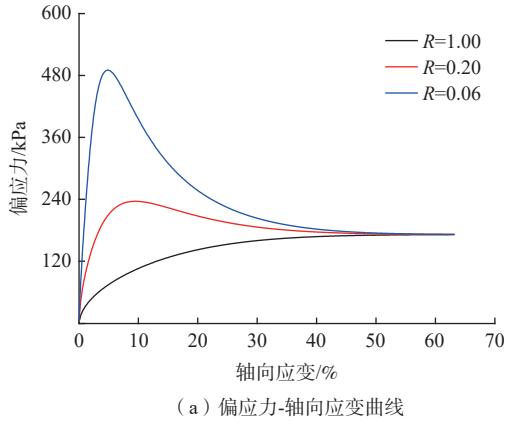


图 3 饱和原状土三轴剪切试验结果与模拟值对比

Fig. 3 Comparison between the results of triaxial shear test of saturated undisturbed soil and the simulated values

表3 算例1—9模型参数表
Table 3 Model parameters of example 1 to 9

算例	λ	$\hat{\kappa}$	μ_0/kPa	α	M	$P_{\text{ref}}/\text{kPa}$	v_{ref}	m	m^*	R	R^*
1	0.11	0.01	200	240	1.1	98	2.23	0.010	0.012	1.00	1.0
2	0.11	0.01	200	240	1.1	98	2.23	0.010	0.012	0.20	1.0
3	0.11	0.01	200	240	1.1	98	2.23	0.010	0.012	0.06	1.0
4	0.11	0.01	200	240	1.1	98	2.23	0.020	0.012	0.11	1.0
5	0.11	0.01	200	240	1.1	98	2.23	0.002	0.012	0.11	1.0
6	0.11	0.01	200	240	1.1	98	2.23	0.010	0.012	1.00	1.0
7	0.11	0.01	200	240	1.1	98	2.23	0.010	0.012	1.00	0.2
8	0.11	0.01	200	240	1.1	98	2.23	0.010	0.002	0.20	0.5
9	0.11	0.01	200	240	1.1	98	2.23	0.010	0.005	0.20	0.5



(a) 偏应力-轴向应变曲线

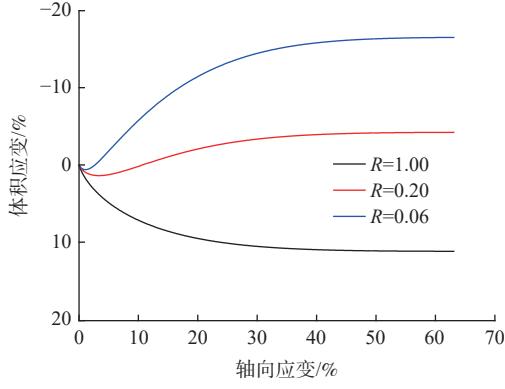


图4 不同初始超固结状态变量计算结果对比

Fig. 4 Comparison of calculated results with different initial overconsolidation state variables

注: 体积应变为正值表示剪缩; 为负值表示剪胀。

度越高。结构性土的三轴固结试验计算结果如图8所示, 从图中可知结构性土 $\ln v - \ln P$ 曲线可超过 NCL; 结构性控制参数越小, $\ln v - \ln P$ 曲线超过 NCL 越明显, 表明在同一应力作用下, 能够承受更大的孔隙比。

4 结论

本文以有限应变理论为框架, 基于超弹性模型和修正剑桥模型, 结合上下负荷面的基本概念和返回映

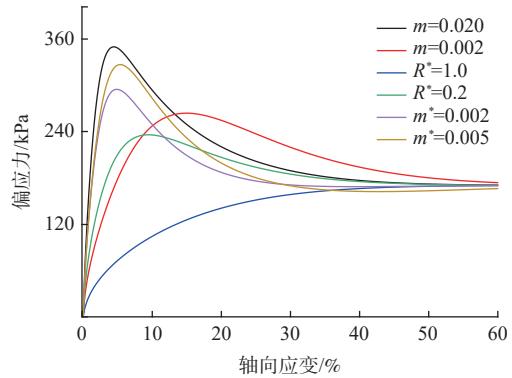


图5 三轴排水剪切试验偏应力-轴向应变曲线

Fig. 5 Deviator stress versus axial strain of the triaxial drained shear test

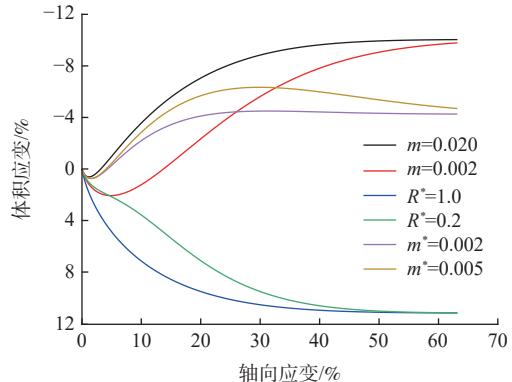


图6 三轴排水剪切试验体积应变-轴向应变曲线

Fig. 6 Volume strain versus axial strain of triaxial drained shear test

射算法, 建立了可描述结构性、超固结和大变形的饱和土有限应变弹塑性本构模型。通过与常规固结试验和等围压三轴排水剪切试验的试验结果进行对比分析, 验证了所提本构模型的正确性。最后通过对三轴等围压排水剪切试验和三轴固结试验的模拟, 讨论了4个模型参数对本构模型的影响。主要结论如下:

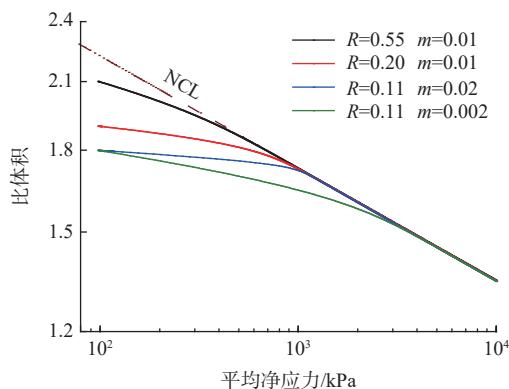


图 7 超固结三轴固结试验计算结果对比

Fig. 7 Comparison of calculated results of triaxial consolidation test of overconsolidation

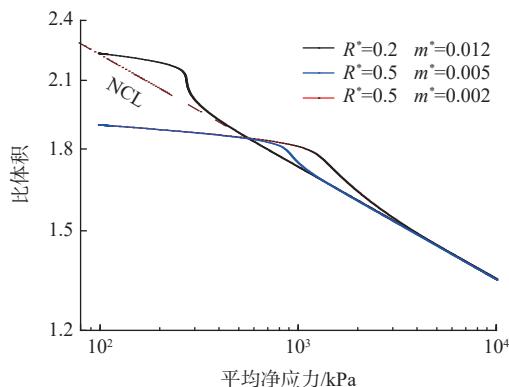


图 8 结构性三轴固结试验计算结果对比

Fig. 8 Comparison of calculated results of structural triaxial consolidation test

(1) 初始超固结比较小的土样发生剪缩, 其表现为应变硬化; 初始超固结比较大的土样先发生剪缩后逐渐发生剪胀, 其表现为先应变硬化而后应变软化。

(2) 随着土体初始结构性的增加, 土体峰值强度显著提升, 其应变软化的程度也有所增大; 随着超固结控制参数的增大, 土体的峰值强度有所上升, 出现峰值强度对应的轴向应变逐渐减小; 随着结构性控制参数越小, 结构性消散越慢, 土体的峰值强度越高。

(3) 不同初始超固结比的 $\ln v - \ln P$ 曲线最终都与正常固结线重合, 超固结控制参数越大, $\ln v - \ln P$ 曲线靠近正常固结线的速度越快。结构性土 $\ln v - \ln P$ 曲线可超过正常固结线; 结构性控制参数越小, $\ln v - \ln P$ 曲线超过正常固结线越明显, 表明在同一应力作用下, 能够承受更大的孔隙比。

所提出的模型在描述土体体变方面仍需要进行改进, 同时将饱和土有限应变弹塑性模型与有限元软件相结合是笔者今后的主要研究内容, 使其更方便地应用到实际工程中去, 从而指导工程实践。

参考文献 (References) :

- [1] 雷升祥, 申艳军, 肖清华, 等. 城市地下空间开发利用现状及未来发展理念 [J]. 地下空间与工程学报, 2019, 15(4): 965 – 979. [LEI Shengxiang, SHEN Yanjun, XIAO Qinghua, et al. Present situations of development and utilization for underground space in cities and new viewpoints for future development[J]. Chinese Journal of Underground Space and Engineering, 2019, 15(4): 965 – 979. (in Chinese with English abstract)]
- [2] 李宏伟, 王国欣. 某地铁站深基坑坍塌事故原因分析与建议 [J]. 施工技术, 2010, 39(3): 56 – 58. [LI Hongwei, WANG Guoxin. Causes and suggestion on deep foundation excavation accident in some metro station[J]. Construction Technology, 2010, 39(3): 56 – 58. (in Chinese with English abstract)]
- [3] 侯艳娟, 张顶立, 李奥. 隧道施工塌方事故分析与控制 [J]. 现代隧道技术, 2018, 55(1): 45 – 52. [HOU Yanjuan, ZHANG Dingli, LI Ao. Analysis and control of collapse events during tunnel construction[J]. Modern Tunnelling Technology, 2018, 55(1): 45 – 52. (in Chinese with English abstract)]
- [4] LU Ning, KHORSHIDI M. Mechanisms for soil-water retention and hysteresis at high suction range[J]. Journal of Geotechnical and Geoenvironmental Engineering, 2015, 141(8): 04015032.
- [5] 朱利君, 裴向军, 张晓超, 等. 双聚材料改良黄土持水性及生态效应研究 [J]. 水文地质工程地质, 2020, 47(4): 158 – 166. [ZHU Lijun, PEI Xiangjun, ZHANG Xiaochao, et al. A study of water retention and ecological effects of loess improved by double polymers[J]. Hydrogeology & Engineering Geology, 2020, 47(4): 158 – 166. (in Chinese with English abstract)]
- [6] 李同录, 张辉, 李萍, 等. 不同沉积环境下马兰黄土孔隙分布与土水特征的模式分析 [J]. 水文地质工程地质, 2020, 47(3): 107 – 114. [LI Tonglu, ZHANG Hui, LI Ping, et al. Mode analysis of pore distribution and soil-water characteristic curve of Malan loess under different depositional environments[J]. Hydrogeology & Engineering Geology, 2020, 47(3): 107 – 114. (in Chinese with English abstract)]
- [7] 赵丹旗, 付昱凯, 侯晓坤, 等. 不同应力路径下饱和重塑黄土的力学特性 [J]. 水文地质工程地质, 2022, 49(6): 74 – 80. [ZHAO Danqi, FU Yukai, HOU Xiaokun, et al. Mechanical properties of saturated remolded loess under different stress paths[J].

- [8] Hydrogeology & Engineering Geology, 2022, 49(6): 74 – 80. (in Chinese with English abstract)]
 [陈家乐, 倪万魁, 王海曼, 等. 原状黄土土-水特征曲线与湿陷性的相关性 [J]. 中国地质灾害与防治学报, 2024, 35(2): 107 – 114. [CHEN Jiale, NI Wankui, WANG Haiman, et al. Correlation between soil-water characteristic curve and collapsibility in undisturbed loess[J]. The Chinese Journal of Geological Hazard and Control, 2024, 35(2): 107 – 114. (in Chinese with English abstract)]]
- [9] Hydrogeology & Engineering Geology, 2022, 49(4): 47 – 54. [CHEN Jiawei, LI Ze, HAN Zhe, et al. Effect of initial void ratio on the soil water characteristics of unsaturated soil at high suctions[J]. Hydrogeology & Engineering Geology, 2022, 49(4): 47 – 54. (in Chinese with English abstract)]
 [陈嘉伟, 李泽, 韩哲, 等. 初始孔隙比对高吸力下非饱和土土水特性的影响 [J]. 水文地质工程地质, 2022, 49(4): 47 – 54. [CHEN Jiawei, LI Ze, HAN Zhe, et al. Effect of initial void ratio on the soil water characteristics of unsaturated soil at high suctions[J]. Hydrogeology & Engineering Geology, 2022, 49(4): 47 – 54. (in Chinese with English abstract)]]
- [10] KADLÍČEK T, JANDA T, ŠEJNOHA M, et al. Automated calibration of advanced soil constitutive models. Part I: Hypoplastic sand[J]. *Acta Geotechnica*, 2022, 17(8): 3421 – 3438.
- [11] MEI Xuan, OLSON S M, HASHASH Y M A. Evaluation of a simplified soil constitutive model considering implied strength and pore-water pressure Generation for one-dimensional (1D) seismic site response[J]. *Canadian Geotechnical Journal*, 2020, 57(7): 974 – 991.
- [12] 岩土工程学报, 2009, 31(10): 1636 – 1641. [LI Guangxin. Some problems in researches on constitutive model of soil[J]. Chinese Journal of Geotechnical Engineering, 2009, 31(10): 1636 – 1641. (in Chinese with English abstract)]
 [李广信. 关于土的本构模型研究的若干问题 [J]. 岩土工程学报, 2009, 31(10): 1636 – 1641. [LI Guangxin. Some problems in researches on constitutive model of soil[J]. Chinese Journal of Geotechnical Engineering, 2009, 31(10): 1636 – 1641. (in Chinese with English abstract)]]
- [13] LIU Qingling, JIAN Wenbin, XU Xutang, et al. A study of the soil-water reliability model in the whole matric suction range[J]. Hydrogeology & Engineering Geology, 2022, 49(1): 92 – 100. (in Chinese with English abstract)]
 [刘青灵, 简文彬, 许旭堂, 等. 基于可靠度方法的全基质吸力段土-水特征模型研究 [J]. 水文地质工程地质, 2022, 49(1): 92 – 100. [LIU Qingling, JIAN Wenbin, XU Xutang, et al. A study of the soil-water reliability model in the whole matric suction range[J]. Hydrogeology & Engineering Geology, 2022, 49(1): 92 – 100. (in Chinese with English abstract)]]
- [14] 岩土工程学报, 2022, 44(4): 678 – 686. [LI Wugang, YANG Qing, LIU Wenhua, et al. Structured quantitative characterization and elastoplastic constitutive model of clay[J]. Chinese Journal of Geotechnical Engineering, 2022, 44(4): 678 – 686. (in Chinese with English abstract)]
 [李吴刚, 杨庆, 刘文化, 等. 黏土的结构性量化表征及其弹塑性本构模型研究 [J]. 岩土工程学报, 2022, 44(4): 678 – 686. [LI Wugang, YANG Qing, LIU Wenhua, et al. Structured quantitative characterization and elastoplastic constitutive model of clay[J]. Chinese Journal of Geotechnical Engineering, 2022, 44(4): 678 – 686. (in Chinese with English abstract)]]
- [15] CHAKRABORTY T, SALGADO R, LOUKIDIS D. A two-surface plasticity model for clay[J]. *Computers and Geotechnics*, 2013, 49: 170 – 190.
 [汪华斌, 周宇, 余刚, 等. 结构性花岗岩残积土三轴试验研究 [J]. 岩土力学, 2021, 42(4): 991 – 1002. [WANG Huabin, ZHOU Yu, YU Gang, et al. A triaxial test study on structural granite residual soil[J]. Rock and Soil Mechanics, 2021, 42(4): 991 – 1002. (in Chinese with English abstract)]
- [16] KONG Lingwei, ZANG Meng, GUO Aiguo, et al. Stress path effect on strength characteristics of Zhanjiang strong structural clay[J]. Rock and Soil Mechanics, 2015(sup 1): 19 – 24. (in Chinese with English abstract)]
 [孔令伟, 臧蒙, 郭爱国, 等. 湛江强结构性黏土强度特性的应力路径效应 [J]. 岩土力学, 2015(增刊1): 19 – 24. [KONG Lingwei, ZANG Meng, GUO Aiguo, et al. Stress path effect on strength characteristics of Zhanjiang strong structural clay[J]. Rock and Soil Mechanics, 2015(sup 1): 19 – 24. (in Chinese with English abstract)]]
- [17] ZHU Enyang, YAO Yangping. A UH constitutive model for structured soils[J]. Rock and Soil Mechanics, 2015, 36(11): 3101 – 3110. (in Chinese with English abstract)]
 [祝恩阳, 姚仰平. 结构性土 UH 模型 [J]. 岩土力学, 2015, 36(11): 3101 – 3110. [ZHU Enyang, YAO Yangping. A UH constitutive model for structured soils[J]. Rock and Soil Mechanics, 2015, 36(11): 3101 – 3110. (in Chinese with English abstract)]]
- [18] ZHU Enyang, YAO Yangping. Constitutively modelling the compression deformation of structured clay[J]. Rock and Soil Mechanics, 2015, 36(7): 1915 – 1922. (in Chinese with English abstract)]
 [祝恩阳, 姚仰平. 结构性土压缩变形本构描述 [J]. 岩土力学, 2015, 36(7): 1915 – 1922. [ZHU Enyang, YAO Yangping. Constitutively modelling the compression deformation of structured clay[J]. Rock and Soil Mechanics, 2015, 36(7): 1915 – 1922. (in Chinese with English abstract)]]
- [19] LU Dechun, LI Xiaoqiang, LIANG Jingyu, et al. 3D elastoplastic constitutive model for normally consolidated soils based on characteristic stress[J]. Chinese Journal of Geotechnical Engineering, 2019, 41(1): 50 – 59. (in Chinese with English abstract)]
 [路德春, 李晓强, 梁靖宇, 等. 基于特征应力的正常固结土三维弹塑性本构模型 [J]. 岩土工程学报, 2019, 41(1): 50 – 59. [LU Dechun, LI Xiaoqiang, LIANG Jingyu, et al. 3D elastoplastic constitutive model for normally consolidated soils based on characteristic stress[J]. Chinese Journal of Geotechnical Engineering, 2019, 41(1): 50 – 59. (in Chinese with English abstract)]]
- [20] LU Dechun, HAN Jiayue, LIANG Jingyu, et al. Non-orthogonal elastoplastic constitutive model of transversely isotropic clay[J]. Chinese Journal of Rock Mechanics and Engineering, 2020, 39(4): 793 – 803. (in Chinese with English abstract)]
 [路德春, 韩佳月, 梁靖宇, 等. 横观各向同性黏土的非正交弹塑性本构模型 [J]. 岩石力学与工程学报, 2020, 39(4): 793 – 803. [LU Dechun, HAN Jiayue, LIANG Jingyu, et al. Non-orthogonal elastoplastic constitutive model of transversely isotropic clay[J]. Chinese Journal of Rock Mechanics and Engineering, 2020, 39(4): 793 – 803. (in Chinese with English abstract)]]
- [21] GUO Wanli, ZHU Jungao, PENG
 [郭万里, 朱俊高, 彭文明. 粗粒土的剪胀方程及广义塑性本构模型研究 [J]. 岩土工程学报, 2018, 40(6): 1103 – 1110. [GUO Wanli, ZHU Jungao, PENG

- [23] 张玉伟, 翁效林, 宋战平, 等. 考虑黄土结构性和各向异性的修正剑桥模型 [J]. 岩土力学, 2019, 40(3): 1030 – 1038. [ZHANG Yuwei, WENG Xiaolin, SONG Zhanping, et al. A modified cam-clay model for structural and anisotropic loess[J]. Rock and Soil Mechanics, 2019, 40(3): 1030 – 1038. (in Chinese with English abstract)]
- [24] BORJA R I. Cam-clay plasticity, part II: Implicit integration of constitutive equation based on a nonlinear elastic stress predictor[J]. Computer Methods in Applied Mechanics and Engineering, 1991, 88(2): 225 – 240.
- [25] HASHIGUCHI K. On the linear relations of $v-\ln p$ and $\ln v-\ln P$ for isotropic consolidation of soils[J]. International Journal for Numerical and Analytical Methods in Geomechanics, 1995, 19(5): 367 – 376.
- [26] BORJA R I, TAMAGNINI C, AMOROSI A. Coupling plasticity and energy-conserving elasticity models for clays[J]. Journal of Geotechnical and Geoenvironmental Engineering, 1997, 123(10): 948 – 957.
- [27] BORJA R I, TAMAGNINI C. Cam-clay plasticity, part III: Extension of the infinitesimal model to include finite strains[J]. Computer Methods in Applied Mechanics and Engineering, 1998, 155(1/2): 73 – 95.
- [28] 胡小荣, 蔡晓峰, 汪日堂. 正常固结饱和黏性土三剪有限变形弹塑性本构模型研究 [J]. 固体力学学报, 2021, 42(2): 156 – 179. [HU Xiaorong, CAI Xiaofeng, WANG Ritang. Approaches to the triple-shear elasto-plastic constitutive models with finite deformations for saturated clays in normal consolidation[J]. Chinese Journal of Solid Mechanics, 2021, 42(2): 156 – 179. (in Chinese with English abstract)]
- [29] 汪俊敏. 地震与降雨耦合作用下边坡渐进性破坏数值分析 [D]. 宁波: 宁波大学, 2021. [WANG Junmin. Numerical analysis of progressive failure of slope under the coupling effect of earthquake and rainfall[D]. Ningbo: Ningbo University, 2021. (in Chinese with English abstract)]
- [30] YE Guanlin, YE Bin. Investigation of the overconsolidation and structural behavior of Shanghai clays by element testing and constitutive modeling[J]. Underground Space, 2016, 1(1): 62 – 77.

编辑: 刘真真